Clays and Clay Minerals, Vol. 55, No. 3, 253–259, 2007.

INHERITANCE *VS.* NEOFORMATION OF KAOLINITE DURING LATERITIC SOIL FORMATION: A CASE STUDY IN THE MIDDLE AMAZON BASIN

ETIENNE BALAN[1,2,*], EMMANUEL FRITSCH[1,2], THIERRY ALLARD[2] AND GEORGES CALAS[2]

[1] IRD-UMR 161 CEREGE, Europole Méditerranéen de l'Arbois BP 80, 13545 Aix-en-Provence cedex, France
[2] Institut de Minéralogie et Physique des Milieux Condensés (IMPMC), UMR CNRS 7590, Université Paris VI, Université Paris VII, IPGP, 4 Place Jussieu, 75252 Paris Cedex 05, France

Abstract—The tropical weathering of sedimentary kaolin deposits from the plateaux surrounding Manaus (Alter do Chao formation, Amazon basin, Brazil) leads to the *in situ* formation of thick kaolinitic soils. The structural changes of kaolinite have been investigated quantitatively by infrared spectroscopy and electron paramagnetic resonance. Both techniques consistently show that each sample contains two types of kaolinite in various proportions. The progressive decrease in kaolinite order from the bottom to the top of the profile results from the gradual replacement of an old population of well-ordered kaolinite, typical of the underlying sedimentary kaolin, by a more recent generation of poorly ordered soil kaolinite. The vertical pattern of kaolinite replacement differs from that of the transformation of Fe oxides and oxy-hydroxides previously observed in the same profile. The inherited fraction of well-ordered kaolinite ranges from 60% at a depth of 9 m to 30% in the upper levels of the soil. The persistence of sedimentary kaolinite in the upper horizons suggests that the rate of kaolinite transformation is relatively slow at the time scale of lateritic soil formation. Kaolinite inheritance unlocks the lateritic record of past weathering conditions.

Key Words—Disorder, EPR, Infrared, Kaolinite, Laterite.

INTRODUCTION

Inheritance *vs.* neoformation of clay minerals during weathering is a central question for understanding soil formation processes and using clays for paleoenvironmental reconstructions (Thiry, 2000). In lateritic profiles, kaolin minerals often display an upward progressive decrease in grain size and crystal order, an indication of the dissolution of old mineral populations accompanied by the crystallization of more recent ones (Tardy, 1993; Tardy and Roquin, 1998). At each level of the soil profiles, inherited and newly formed kaolinite crystals are thus expected to occur, the proportion being directly determined by the rate of mineral transformation. Depending on the assumptions made about dissolution and precipitation rates, different interpretations concerning the dynamics of the whole lateritic profile can be inferred from the observed transformations. In a model assuming rapid dissolution-crystallization cycles and relatively large water/rock ratios, referred to as the "dynamical equilibrium" model, the inherited fraction is small (Lucas *et al.*, 1993, 1996). The crystal-chemical properties and isotopic composition of kaolinite (Giral-Kacmarcik *et al.*, 1998) are then considered representative of the physical-chemical conditions prevailing in soil micro-environments at the present time. In this model, the heterogeneity of kaolinite populations may be attributed to variations of these physicochemical conditions in space (*e.g.* coexistence of various local micro-environments) and/or time (e.g. seasonal changes). Alternatively, in a model assuming slow dissolution-crystallization processes, the inherited fraction may be significant. In this case, the progressive change in crystal-chemical properties observed from bottom to top may simply reflect the progressive transformation of an old kaolinite population to a more recent one. The observed variations are explained by variations in the advancement of a forward transformation reaction and not by a dynamic equilibrium with varying local conditions. The relative resistance of kaolinite to transformation then supports the use of its isotopic composition for paleoclimatic investigations (Girard *et al.*, 2000).

In the middle part of the Amazon basin (Manaus region, Brazil), sedimentary kaolin deposits have been exposed to long-term tropical weathering processes, leading to the *in situ* formation of thick lateritic soils. This type of profile is thus ideally suited to investigate the resistance of kaolinite to changes in physicochemical conditions. Except for an intermediate horizon displaying hematitic nodules, the loose materials reveal progressive chemical changes as well as a progressive decrease in the kaolinite order from bottom to top. These progressive changes have previously been considered as evidence for the "dynamical equilibrium" of kaolinites along the profiles, implying a major contribution of kaolinite in the Si biogeochemical cycle (Lucas *et al.*, 1993, 1996). In this study, we show that a model based on only two kaolinite populations with differing structural order accounts for the structural modifications of kaolinite at a molecular scale. The interlayer

* E-mail address of corresponding author:
Etienne.Balan@impmc.jussieu.fr
DOI: 10.1346/CCMN.2007.0550303

configuration is probed by the stretching vibrations of OH groups in the infrared (IR) spectra. The distortions affecting the internal structure of the dioctahedral layer are investigated by the electron paramagnetic resonance (EPR) signal of structural Fe^{3+} ions substituted for Al^{3+} ions in octahedral sites.

GEOLOGICAL SETTINGS AND SAMPLING

The geological context has been described extensively in previous works (Fritsch *et al.*, 2002, 2005). The soils are developed on the thick continental sediments of the middle Amazon basin (Alter do Chao formation). The sediments consist of sandy clay deposits with sand intercalations and cross-bedded stratifications. Their mineralogy is dominated by quartz and kaolinite but also includes hematite, goethite, Ti oxides and zircon. Observation of well-formed kaolinite booklets indicates extensive crystallization of kaolinite after sediment deposition (Lucas *et al.*, 1996). Quartz dissolution and an upwards increase in clay content correspond to the gradual disappearance of sedimentary structures and the appearance of soil horizons.

The soil horizons were sampled on a 10 m thick cross-section at a road cut, located at the edge of a plateau ~4 km north of the town of Manaus (Figure 1). The mineralogical and chemical characteristics of the profile under study were reported by Fritsch *et al.* (2002, 2005). A thin line of hematitic gravels delineates an abrupt discontinuity in the vertical soil differentiation. According to Lucas *et al.* (1990), the hematitic stone lines observed in the Manaus area probably result from the thinning of a previously thick nodular horizon and *in situ* accumulation of gravel-size nodules in a thin residual layer. Seven loose soil samples were collected in profile I (Table 1). Two samples correspond to subsoil horizons (I-9.10, I-7.15), one to the loose soil matrix surrounding the hematitic gravels of the stone line (I-5.70) and four to topsoil horizons (I-4.10, I-2.80, I-1.10, I-0.50). Note that sample I-9.10 located at the bottom of the investigated profile does not correspond to the parent sedimentary rock but already displays soil features, such as a reddish pink color and micro-aggregation (Fritsch *et al.*, 2002).

Two reference samples of kaolinite, referred to as A1 and B4 (Balan *et al.*, 1999, 2000, 2005a), were also used to interpret the spectroscopic data. These samples originate from a nearby thicker lateritic profile described by Lucas *et al.* (1996). The A1 sample corresponds to a well-ordered kaolinite sample and is typical of the underlying sedimentary horizons (Balan *et al.*, 2005a). In contrast, the B4 sample is representative of the highest degree of stacking disorder found in the lateritic soils of the Manaus area (Giral-Kacmarcik *et al.*, 1998; Balan *et al.*, 2005a). Disordered samples with similar EPR spectra have also been observed in top horizons of lateritic profiles from the Jari river area (Montes-Lauar *et al.*, 2002) and pedogenic kaolin from Minas Gerais (Varajão *et al.*, 2001).

EXPERIMENTAL METHODS

The samples were air dried, sieved to pass 2 mm and homogenized prior to analysis. Chemical composition was determined by inductively coupled plasma atomic emission spectrometry for major elements (Al, Si, Fe, Ti) (Fritsch *et al.*, 2005). To improve the quality of EPR spectra, a dithionite-citrate-bicarbonate (DCB) treatment (Mehra and Jackson, 1960) was performed to remove most of the Fe oxides.

The EPR measurements at 9.42 GHz (X-band) were performed at room temperature using a Bruker ESP300E

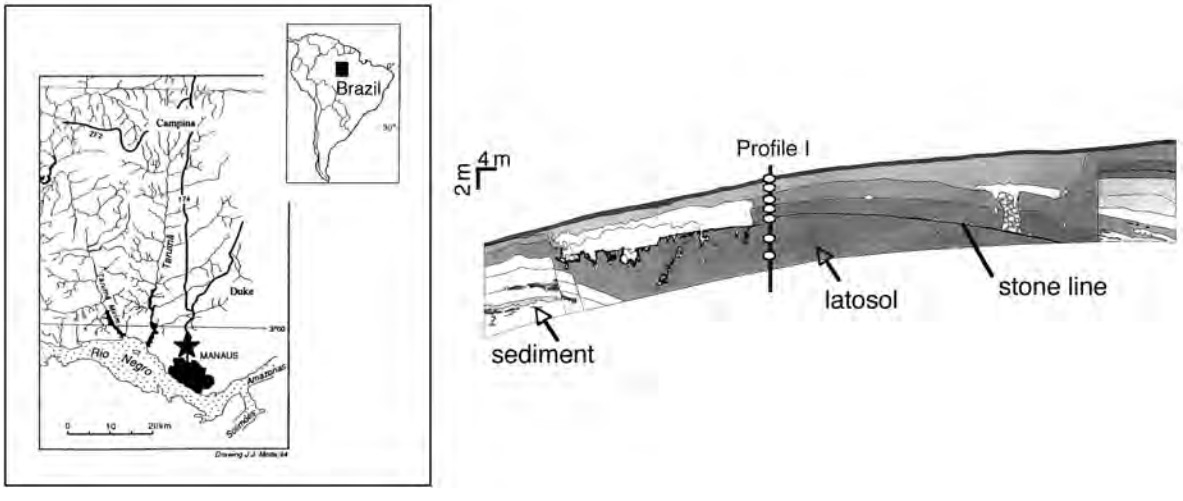

Figure 1. Location and cross-sections of the profile (after Fritsch *et al.*, 2002). Sedimentary and soil structures were delimited from photocomposition and field observations.

Table 1. Mineralogical composition of the samples.

Sample	Depth (m)	Ti oxides (wt.%)	Fe oxides (wt.%)	Gibbsite (wt.%)	Quartz (wt.%)	Kaolinite (wt.%)	Fraction of low-order kaolinite IR	EPR
I050	0.50	1.7	3.9	1.4	29.4	63.7	0.67	0.71
I110	1.10	1.7	4.0	1.6	23.1	69.6	0.66	0.69
I280	2.80	1.7	3.8	3.4	14.0	77.2	0.68	0.70
I410	4.10	1.6	3.3	1.0	14.8	79.3	0.68	0.67
I570	5.70	1.4	2.8	1.2	23.3	71.3	0.61	0.58
I715	7.15	1.3	2.1	0.0	29.6	67.0	0.54	0.52
I910	9.10	1.0	1.3	0.4	46.9	56.4	0.38	0.36

spectrometer. All spectra were recorded using the same measurement parameters (microwave power = 40 mW, frequency of modulation = 100 kHz, amplitude of modulation = 5 G), while the gain depended on the sample. No saturation of the paramagnetic Fe^{3+} signal was observed, increasing the microwave power to 200 mW. Powder samples (~40 mg) were placed in pure silica tubes (Suprasil grade). In order to ensure reliability of quantitative intensity measurements, the silica tubes were filled with constant volume and carefully inserted at the same place in the resonance cavity (Balan *et al.*, 2000). Experimental spectra were normalized with respect to gain, sample weight and kaolinite content.

To record IR spectra, ~1 mg of sample was gently ground with 300 mg of KBr. The mixture was pressed to produce a KBr pellet and the transmission IR spectrum of the pellet was recorded at room temperature using a Nicolet Magna 560 FTIR spectrometer with a resolution of 2 cm^{-1}.

RESULTS

Electron paramagnetic resonance

Full-range EPR spectra of selected kaolinite samples (A1, B4, I-050, I-940) were reported in a previous study (Balan *et al.*, 2005a). Here, we focus on the signals around 0.16 T which are related to dilute Fe^{3+} ions substituted for Al^{3+} ions within the octahedral sheet of kaolinite (Figure 2). Depending on the sample, two contributions referred to as Fe_I and Fe_{II} can be identified: a nearly isotropic signal (Fe_I) centered at 0.16 T and an anisotropic signal (Fe_{II}) with resonances near 0.136 T and 0.180 T.

The EPR spectrum of the sedimentary reference sample (A1) mostly displays an Fe_{II} type spectrum (Figure 2). This spectrum can be modeled using two sets of fine structure parameters related to the two axially distorted Al sites in ordered kaolinite (Balan *et al.*, 1999). In contrast, the spectrum of the topsoil reference sample (B4) mostly exhibits an Fe_I type spectrum (Figure 2). A detailed EPR study performed at X-band and Q-band frequencies has shown that this spectrum is also related to trivalent Fe ions substituted for Al in the octahedral sheets of the kaolinite structure (Balan *et al.*, 1999). However, its interpretation requires consideration of a continuous distribution of fine structure parameters instead of two discrete sets for the Fe_{II} type spectrum. The Fe_I signal is in fact produced by changes of the symmetry of octahedral sites owing to the random distribution of the vacant site in successive layers. The shape of this distribution suggests the occurrence of dickite-like stacking domains produced by a high proportion of stacking faults in the disordered B4 sample (Balan *et al.*, 1999). Therefore, the relative

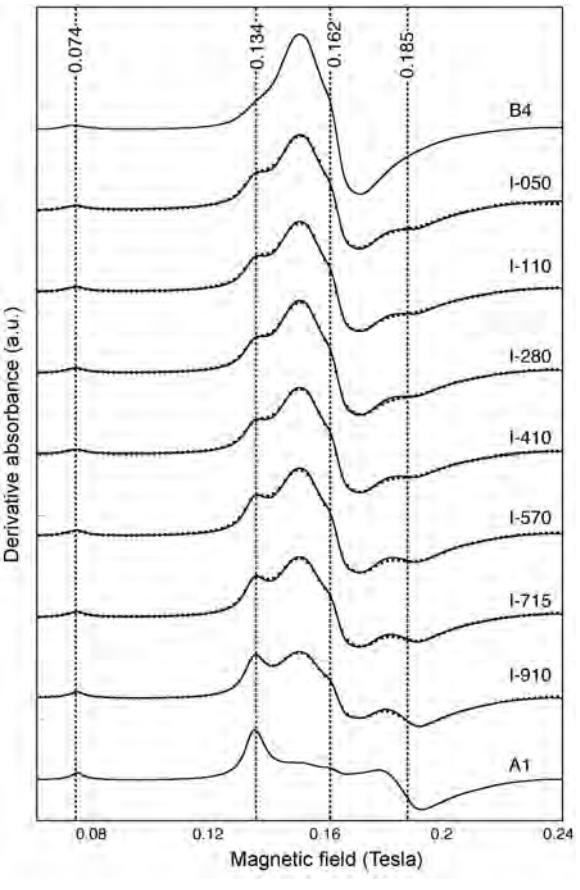

Figure 2. X-band EPR spectra of the investigated series. Points – experiment; continuous line – fit. The spectra have been fitted (Rp ≈ 4.2%) using the spectrum of reference samples A1 (bottom) and B4 (top).

contribution of the Fe_{II} and Fe_{I} signal can be correlated to the stacking order of kaolinite, provided that the distribution of Fe^{3+} ions within the kaolinite structure is homogeneous.

Spectra related to the loose horizons of the profile I display intermediate shape with both the Fe_{I} and Fe_{II} type signals (Figure 2). From bottom to top, the relative intensity of the resonances ascribed to the Fe_{II} spectrum decreases progressively, indicating an overall decrease in the stacking order of kaolinites. The spectra were least-squares fitted using the reference spectra of samples A1 and B4, which present almost pure Fe_{II} and Fe_{I} signals, respectively. A linear baseline accounting for the slope related to the large superparamagnetic signal centered at 0.3 T resulted in good fits (Figure 2). The proportion of B4-type spectrum increases progressively from bottom to a depth of 4 m and remains almost constant above (Figure 3). The change in the shape of the Fe^{3+} EPR signal does not correspond to a significant variation of the structural Fe^{3+} content of the kaolinite. In fact, the Fe concentration assessed from the intensity of the EPR spectra ranges between 2300 and 2800 ppm, which is close to that observed in A1 and B4 (2800 ppm) (Balan *et al.*, 2000).

Infrared spectroscopy

The spectrum of sample A1 is characteristic of a well-ordered sample (Figure 4). Besides the band at 3619 cm^{-1} related to the stretching vibration of the inner OH group, it displays three bands at 3652, 3668 and 3695 cm^{-1}. These bands correspond to the two out-of-phase and the in-phase motion modes of inner-surface OH groups (Balan *et al.*, 2001). A weak band is also observed at 3597 cm^{-1}. It corresponds to an Fe,Al-OH stretching band and indicates the presence of Fe^{3+} ions substituted in the octahedral sheet of the kaolinite structure (Petit *et al.*, 1990; Delineau *et al.*, 1994; Iriarte *et al.*, 2005). The spectrum of sample B4 differs significantly from that of A1 (Figure 4). The strong bands on the low- and high-frequency sides of the spectrum are broadened and shifted slightly at 3621 and 3700 cm^{-1}, respectively, in the B4 spectrum. The two central bands are replaced by an intense and broad band observed at 3650 cm^{-1}. In fact, the spectrum of sample B4 has significant similarities to the spectrum of dickite (Farmer, 1974; Prost *et al.*, 1989). This change is related to the rotation of the inner-surface OH group facing the inner OH group. In the kaolinite structure, this inner-surface OH group is nearly perpendicular to the *a*,*b* plane whereas it is inclined in the dickite structure. The two configurations are nearly isoenergetic but lead to markedly different IR spectra because the rotation of the OH group prevents its motion being coupled with that of the two other inner-surface OH groups (Balan *et al.*,

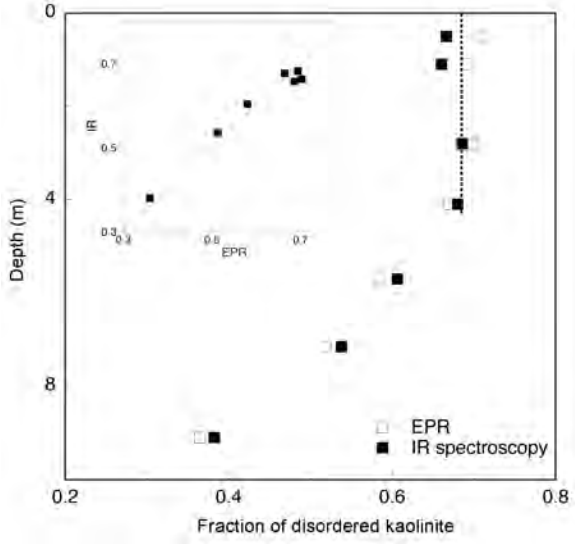

Figure 3. Proportion of disordered kaolinite as a function of depth. This proportion corresponds to the fraction of B4-type spectrum used to fit the IR (filled squares) or EPR (open squares) spectra. The two techniques provide quantitatively consistent results (inset).

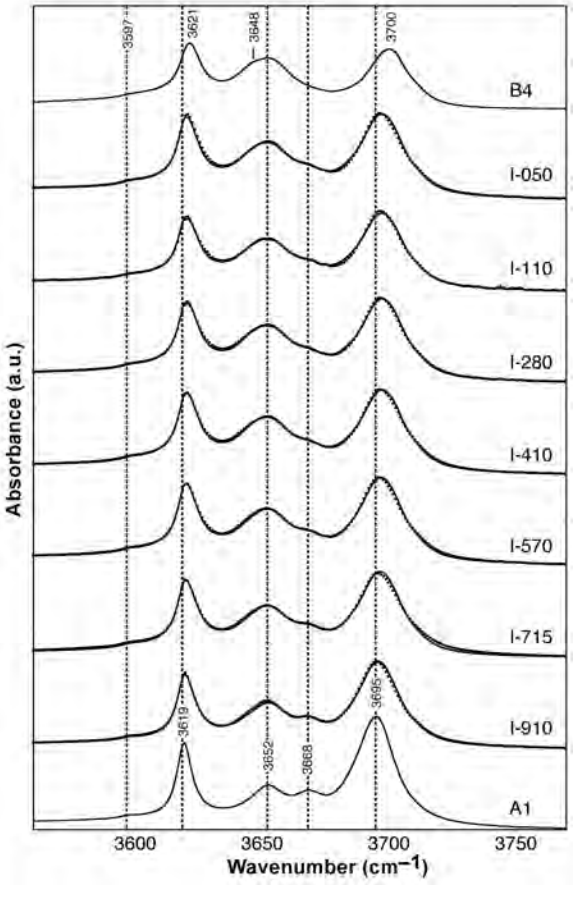

Figure 4. Powder transmission IR spectra of the investigated series. Points – experiment; continuous line – fit. The spectra were fitted (Rp ≈ 3.5%) using the spectrum of reference samples A1 (bottom) and B4 (top).

2005b). The occurrence of a dickite-like hydroxyl configuration in sample B4, also inferred from EPR data, is probably related to stacking faults, in which the normal translation between two adjacent layers is replaced by a glide plane. This kind of stacking fault will be referred to as a dickite-like stacking domain in the present study. Note that the blue shift of the band at 3700 cm^{-1} in the IR spectrum may also be partly related to the smaller thickness of kaolinite particles (Balan *et al.*, 2001). The weak band at 3597 cm^{-1} ascribed to Fe^{3+} ions isomorphously substituted for Al^{3+} ions is still present in the spectrum but slightly broadened.

Similar to the observations obtained by EPR spectroscopy, the IR spectra of the loose horizons are intermediate between that of the A1 and B4 samples (Figure 4). In particular, from bottom to top, the relative intensity of the band at 3668 cm^{-1} decreases progressively and the two intense absorption bands are slightly shifted and broadened. Therefore, the spectra were least-squares fitted using the reference spectra of samples A1 and B4 (Figure 4). A linear baseline accounting for the slope related to traces of adsorbed water and minor quantity of other hydrous phases was used and good fits were obtained (Figure 4).

A good agreement is observed between the proportions derived using IR spectroscopy and those derived using the EPR spectra of substituted Fe^{3+} ions (Figure 3). Such consistency supports the interpretation of the Fe_I EPR signal of sample B4 in terms of distortions of the 1:1 layer related to dickite-like configurations (Balan *et al.*, 1999).

DISCUSSION

Fe distribution and kaolinite order

The similarity between the proportion of disordered kaolinite assessed using the EPR signal of isolated structural Fe^{3+} ions and that determined using the OH-stretching bands in IR spectra provides important information about the distribution of Fe^{3+} ions in kaolinite particles. Indeed, it shows that Fe ions probe the same amount of stacking faults as OH groups, implying that the distribution of Fe ions is homogeneous within the particles. Therefore, the proportion of Fe^{3+} ions located near a stacking fault is similar to that occurring in normally stacked layers. This is an indication that the formation of stacking faults in the investigated kaolinite samples is not related to the occurrence of structural Fe^{3+} ions as previously observed in other series of kaolinite samples (e.g. Brindley *et al.*, 1986; Stone and Torres-Sanchez, 1988; Petit and Decarreau, 1990; Balan *et al.*, 2000). Consequently, the EPR spectrum of homogeneously distributed Fe^{3+} ions is an efficient probe of kaolinite order. Interestingly, the elevated proportion of dickite-like stacking configurations seems to be quite specific to the kaolinites developed on the Alter do Chao formation of the middle Amazon basin. Other disordered kaolinites, such as those from Georgia (KGa-2) (Balan *et al.*, 2000) or Charente basin (France) sediments (Balan *et al.*, 1999) or from the lateritic soil of Goyoum (Cameroon) (Muller and Bocquier, 1987) have a different Fe_I spectrum. The latter corresponds to a different distribution of fine-structure parameters (Balan *et al.*, 1999) and suggests the predominance of a different type of stacking faults in these disordered kaolinites. Beside dickite-like stacking configuration, these stacking faults may include layer rotation (±120º), layer translation (±*b*/3 shift) or occurrence of enantiomeric layers (*e.g.* Giese, 1988; Bookin *et al.*, 1989; Plançon *et al.*, 1989; Artioli *et al.*, 1995; Kogure and Inoue, 2005).

Neoformation of kaolinites and geochemical evolution of the lateritic profile

The EPR and IR spectra indicate a decrease in kaolinite order from the bottom to the top of the profile, which arises together with a decrease in the size of kaolinite particles (Fritsch *et al.*, 2002). In fact, the spectra can be fitted efficiently using just two reference spectra corresponding to an ordered and a disordered type of kaolinite; both spectroscopic methods providing quantitatively consistent results (Figure 3). This strongly suggests that the samples can be considered as a mixture of two types of kaolinite, the ordered one prevailing in the sediment-dominated samples and the disordered one being specific to the lateritic soil. Up to a depth of 4 m, the kaolinite content of the samples is correlated to the concentration in weakly mobile elements such as Ti, Zr or Th (Table 1; see also Fritsch *et al.*, 2002). Accordingly, the progressive structural changes affecting kaolinite in the profile occur without kaolinite loss. They result from the upwards replacement of an old population of kaolinite formed in the sedimentary horizons, characterized by a small amount of stacking faults and large particle size, by a more recent one formed in lateritic soils, with a large number of stacking faults and smaller particle size. Note that the coexistence of two populations of kaolinites in a given sample does not imply that these populations can be physically separated because pre-existing particles may act as templates for the growth of the new population.

Inheritance of kaolinite is significant all along the profile. The topsoil horizons still contain ~20 wt.% of inherited ordered kaolinite and 45 wt.% of disordered kaolinite, indicating that the kaolinite replacement is not complete even in the uppermost horizon of the profile. The linear decrease of the ordered kaolinite fraction as a function of decreasing depth (Figure 5) suggests that the dissolution of the initial population of kaolinite occurs at a steady rate all along the profile. In the subsoil horizon, this dissolution is compensated by the precipitation of disordered kaolinites. Whereas water-saturated conditions controlled the growth of well-ordered kaolinites in

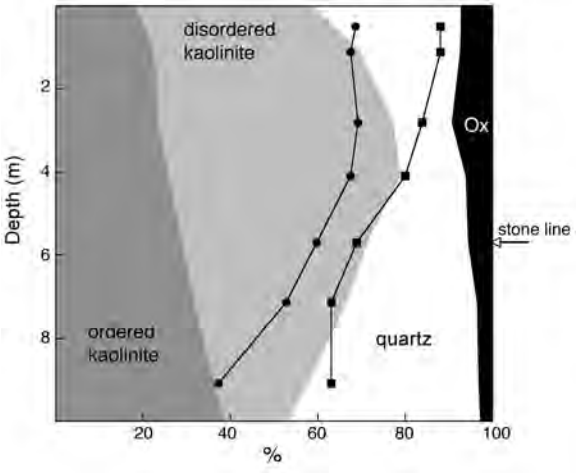

Figure 5. Mineralogical composition (wt.%) of the investigated samples displaying the contributions of ordered and disordered kaolinites. The fraction of kaolinite corresponding to the disordered type (circles), as well as the fraction of Fe oxide corresponding to goethite (squares) (Fritsch *et al.*, 2005) are reported. Ox – Ti, Al and Fe (hydr)oxides.

the sedimentary horizons, the formation of disordered kaolinite in the soils indicate fluctuations of physical-chemical conditions leading to transitory high-affinity conditions for the precipitation reaction. The increasing proportion of disordered kaolinite and the dissolution of quartz lead to a relative accumulation of kaolinite. In contrast, in the topsoil horizons (from a depth of ~4 m to the surface), dissolution of kaolinite prevails and quartz starts to concentrate. As the ratio of disordered to ordered kaolinites is almost constant in these horizons (Figure 3), the dissolution of ordered and disordered kaolinites should occur at a similar rate.

Therefore, a neoformation model assuming rapid dissolution-crystallization cycles affecting kaolinites may be inappropriate to describe the evolution of the lateritic profile. Instead, the variations in the mean characteristics of kaolinite samples can be explained by the increasing advancement from the bottom to the top of the profile of a single replacement reaction. The apparent age of kaolinites in the investigated profile has been estimated from their radiation-induced paramagnetic defects (Balan *et al.*, 2005a). It decreases from 17 to 8 Ma from sample I-910 to sample I-050, consistent with an ancient transformation of kaolinites. However, the significant apparent age determined for the topsoil kaolinites in lateritic covers of the Manaus area can also be interpreted as the residence time of disordered kaolinite particles in the soil, indicating a slow evolution of the disordered population of kaolinites through dissolution-precipitation cycles.

The stone line, which appears as a major structural discontinuity of the investigated profile at ~5.7 m, does not affect the transformations occurring in the loose soil matrix. Its formation is thus probably related to older weathering processes. Similar observations have been made on kaolinites from nodules present in Cameroon laterites which have preserved reduced species (Mn^{2+}) under oxidizing conditions (Muller and Calas, 1993).

A comparison can be carried out between the evolution of kaolinite in the investigated lateritic profile and that of the finely divided Fe oxides and oxy-hydroxides. The mineralogical changes affecting Fe oxides in the profile have been interpreted as the replacement of older populations of hematite and goethite by a younger population of aluminous goethite, through dissolution and precipitation processes and without Fe loss (Fritsch *et al.*, 2005). As observed above, kaolinite replacement mainly occurs in the subsoil, whereas kaolinite dissolution and Fe oxide replacement prevails in the topsoil (Figure 5). The contrasted trends observed between kaolinite and Fe oxides suggest distinct evolutions in space and time. In fact, during the replacement of kaolinite, Fe^{3+} is weakly mobile, explaining why the disordered kaolinites observed in the soil have a structural Fe content similar to that of the underlying ordered kaolinites. In contrast, the Al enrichment of goethite, together with the formation of a minor quantity of gibbsite in the topsoil horizons, have been related to the dissolution of kaolinites (Fritsch *et al.*, 2002, 2005). These observations are consistent with the overprinting of three stages of evolution in the investigated profile. The most ancient stage only appears as a relict stone line of hematitic nodules. The intermediate stage corresponds to the relative accumulation of kaolinite occurring simultaneously with the replacement of ordered kaolinites by disordered ones. The last stage corresponds to the transformation of Fe oxides and dissolution of kaolinite, which leads to the accumulation of aluminous goethite and the formation of gibbsite. This last stage is probably related to the present-day weathering conditions prevailing in the middle Amazon basin.

CONCLUSIONS

Our results indicate that kaolinite is relatively resistant to low-temperature dissolution under tropical weathering conditions. Spectroscopic methods sensitive to the local structural order of crystals may contribute significantly to the identification and quantification of the various populations of kaolinite co-existing in a given lateritic profile. This observation is probably not restricted to profiles developed on sedimentary rocks because the upper horizons of many lateritic profiles are formed at the expense of older kaolinite-rich saprolitic horizons. However, these kaolinites may suffer significant changes in grain size and morphology, making it difficult to assess their occurrence in the topsoil horizons. In any case, kaolinite inheritance will unlock the record of past weathering conditions during laterite formation.

ACKNOWLEDGMENTS

We thank S. Petit (HydrASA-Poitiers) and two anonymous reviewers for their helpful comments. Marie Dreano and Alexia Chandor (ENSCP, Paris) and Yanling Li (LMCP, Paris) are acknowledged for their contribution to the IR measurements. This work was supported by the French National Research Agency (ANR project SPIRSE). This is IPGP contribution 2194.

REFERENCES

Artioli, G., Bellotto, M., Gualtieri, A. and Pavese, A. (1995) Nature of structural disorder in natural kaolinites: a new model based on computer simulation of powder diffraction data and electrostatic energy calculation. *Clays and Clay Minerals*, **43**, 438–445.

Balan, E., Allard, T., Boizot, B., Morin, G. and Muller, J.-P. (1999) Structural Fe^{3+} in natural kaolinites: New insights from electron paramagnetic resonance spectra fitting at X and Q-band frequencies. *Clays and Clay Minerals*, **47**, 605–616.

Balan, E., Allard, T., Boizot, B., Morin, G. and Muller, J.-P. (2000) Concentration of paramagnetic structural Fe(+III) in natural kaolinites. *Clays and Clay Minerals*, **48,** 439–445.

Balan, E., Saitta, A.M., Mauri, F. and Calas, G. (2001) First-principles modeling of the infra-red spectrum of kaolinite. *American Mineralogist*, **86**, 1321–1330.

Balan, E., Allard, T., Fritsch, E., Sélo, M., Falguères, C., Chabaux, F., Pierret, M.-C. and Calas, G. (2005a) Formation and evolution of lateritic profiles in the middle Amazon basin: Insights from radiation-induced defects in kaolinite, *Geochimica et Cosmochimica Acta*, **69**, 2193–2204.

Balan, E., Lazzeri, M., Saitta, A.M., Allard, T., Fuchs, Y. and Mauri, F. (2005b) First-principles study of OH stretching modes in kaolinite, dickite and nacrite. *American Mineralogist*, **90**, 50–60.

Bookin, A.S., Drits, V.A., Plançon, A. and Tchoubar, C. (1989) Stacking faults in kaolin-group minerals in the light of real structural features. *Clays and Clay Minerals*, **37**, 297–307.

Brindley, G.W., Kao, C.-C., Harrison, J.L., Lipsicas, M. and Raythatha, R. (1986) Relation between structural disorder and other characteristics of kaolinites and dickites. *Clays and Clay Minerals*, **34**, 239–249.

Delineau, T., Allard, T., Muller, J-P., Barres, O., Yvon, J. and Cases, J.-M. (1994) FTIR reflectance *vs.* EPR studies of structural iron in kaolinites. *Clays and Clay Minerals*, **42**, 308–320.

Farmer, V.C. (1974) *The Infrared Spectra of Minerals*. Mineralogical society, London.

Fritsch, E., Montes-Lauar, C.R., Boulet, R., Melfi, A.J., Balan, E. and Magat, Ph. (2002) Lateritic and redoximorphic features in fractured soils and sediments of the Manaus plateaus, Brazil. *European Journal of Soil Science*, **53**, 203–218.

Fritsch, E., Morin, G., Bedidi, A., Bonnin, D., Balan, E., Caquineau, S. and Calas, G. (2005) Transformation of haematite and Al-poor goethite to Al-rich goethite and associated yellowing in a ferralitic clay soil profile of the middle Amazon basin (Manaus, Brazil). *European Journal of Soil Science*, **56**, 575–588.

Giese, R.F., Jr. (1988) Kaolin minerals: structures and stabilities. Pp. 29–66 in: *Hydrous Phyllosilicates (Exclusive of Micas)* (S.W. Bailey, editor). Reviews in Mineralogy, vol. **19**. Mineralogical Society of America, Washington, D.C.

Giral-Kacmarcik, S., Savin, S.M., Nahon, D.B., Girard, J.-P., Lucas, Y. and Abel, L. (1998) Oxygen isotope geochemistry of kaolinite in laterite-forming processes, Manaus, Amazonas, Brazil. *Geochimica et Cosmochimica Acta*, **62**, 1865–1879.

Girard, J.-P., Freyssinet, Ph. and Chazot, G. (2000) Unraveling climatic changes from intraprofile variation in oxygen and hydrogen isotopic compositions of goethite and kaolinite in laterites: An integrated study from Yaou, French Guiana. *Geochimica et Cosmochimica Acta*, **64**, 409–426.

Iriarte, I., Petit, S., Javier Huertas, F., Fiore, S., Grauby, O., Decarreau, A. and Linares, J. (2005) Synthesis of kaolinite with a high level of Fe^{3+} for Al substitution. *Clays and Clay Minerals*, **53**, 1–10.

Kogure, T. and Inoue, A. (2005) Determination of defect structure in kaolin minerals by high-resolution transmission electron microscopy. *American Mineralogist*, **90**, 85–89.

Lucas, Y., Boulet, R. and Chauvel, A. (1990) In situ genesis of stone lines. Demonstrative example from a lateritic cover in Brazilian Amazonia. *Comptes Rendus de l'Académie des Sciences de Paris*, **311**, 713–718.

Lucas, Y., Luizão, F.J., Chauvel, A., Rouiller, J. and Nahon, D. (1993) The relation between biological activity of the rain forest and mineral composition of soils. *Science*, **260,** 521–523.

Lucas, Y., Nahon, D., Cornu, S. and Eyrolle, F. (1996) Genèse et fonctionnement des sols en milieu équatorial. *Comptes Rendus de l'Académie des Sciences de Paris*, **322**, 1–16.

Mehra, O.P. and Jackson, M.L. (1960) Fe oxide removal from soil and clays by a dithionite-citrate system buffered with sodium carbonate. *Clays and Clay Minerals*, **7**, 317–327.

Muller, J.P. and Bocquier, G. (1987) Textural and mineralogical relationships betweeen ferruginous nodules and surrounding clayey matrices in a laterite from Cameroon. Pp. 186–196 in: *Proceedings of the International Clay Conference, Denver, 1985* (L.G. Schultz, H. van Olphen and F.A. Mumpton, editors). The Clay Minerals Society, Bloomington, Indiana.

Muller, J.P. and Calas G. (1993) Mn^{2+}-bearing kaolinites from lateritic weathering profiles: geochemical significance. *Geochimica et Cosmochimica Acta*, **57**, 1029–1037.

Petit, S. and Decarreau, A. (1990) Hydrothermal (200ºC) synthesis and crystal chemistry of iron-rich kaolinites. *Clay Minerals*, **25**, 181–196.

Plançon, A., Giese, R.F., Snyder, R., Drits, V.A. and Bookin, A.S. (1989) Stacking faults in the kaolin-group minerals: The defect structure of kaolinite. *Clays and Clay Minerals*, **37**, 203–210.

Prost, R., Damene, A., Huard, E., Driard, J. and Leydecker, J.P. (1989) Infrared study of structural OH in kaolinite, dickite, nacrite and poorly crystalline kaolinite at 5 to 600 K. *Clays and Clay Minerals*, **37**, 464–468.

Stone, W.E.E. and Torres-Sanchez, R.M. (1988) Nuclear magnetic resonance spectroscopy applied to minerals. Part 6. Structural iron in kaolinites as viewed by proton magnetic resonance. *Journal of the Chemical Society, Faraday Transactions I*, **84**, 117–132.

Tardy, Y. (1993) *Pétrologie des Latérites et des Sols Tropicaux*. Masson, Paris.

Tardy, Y. and Roquin, C. (1998) *Dérive des Continents. Paléoclimats et Altérations Tropicales*. Editions BRGM, Orléans, France, 469 pp.

Thiry, M. (2000) Palaeoclimatic interpretation of clay minerals in marine deposits: an outlook from the continental origin. *Earth-Science Reviews*, **49**, 201–221.

Varajão, A.F.D.C., Gilkes, R.J. and Hart, R.D. (2001) The relationships between kaolinite crystal properties and the origin of materials for a brazilian kaolin deposit. *Clays and Clay Minerals*, **49**, 44–59.

(*Received 29 September 2006; revised 20 December 2006; Ms. 1222; A.E. Bruno Lanson*)